

Accelerating the discovery of novel magnetic materials using machine learning-guided adaptive feedback

Weiyi Xia^{a,b}, Masahiro Sakurai^{c,d}, Balamurugan Balasubramanian^{e,f}, Timothy Liao^{c,g}, Renhai Wang^{a,h}, Chao Zhangⁱ, Huaijun Sun^j, Kai-Ming Ho^a, James R. Chelikowsky^{c,g,k,1}, David J. Sellmyer^{e,f,2}, and Cai-Zhuang Wang^{a,b,1}

Edited by Erio Tosatti, Scuola Internazionale Superiore di Studi Avanzati, Trieste, Italy; received March 14, 2022; accepted October 5, 2022

Magnetic materials are essential for energy generation and information devices, and they play an important role in advanced technologies and green energy economies. Currently, the most widely used magnets contain rare earth (RE) elements. An outstanding challenge of notable scientific interest is the discovery and synthesis of novel magnetic materials without RE elements that meet the performance and cost goals for advanced electromagnetic devices. Here, we report our discovery and synthesis of an RE-free magnetic compound, Fe₃CoB₂, through an efficient feedback framework by integrating machine learning (ML), an adaptive genetic algorithm, first-principles calculations, and experimental synthesis. Magnetic measurements show that Fe₃CoB₂ exhibits a high magnetic anisotropy ($K_1 = 1.2 \text{ MJ/m}^3$) and saturation magnetic polarization $(J_s = 1.39 \text{ T})$, which is suitable for RE-free permanent-magnet applications. Our ML-guided approach presents a promising paradigm for efficient materials design and discovery and can also be applied to the search for other functional materials.

magnetic materials | materials discovery | machine learning | methodology development

Computational-driven discovery of novel materials with targeted functionalities is a highly active research area owing to rapid advances in computer and communication technologies, machine learning (ML) algorithms, and data sciences. For accelerating the speed of materials discovery, it is essential to efficiently establish the relationships among chemical compositions, crystal structures, and physical properties. In the past few decades, several efficient computational algorithms including an adaptive genetic algorithm (AGA) have been developed to predict stable crystal structures based on given chemical compositions (1–4). These algorithms and methods are very useful in guiding materials discovery (5-7). However, the number of possible combinations of different elements with different compositions, and the crystal structures that they may adopt, is enormous, especially for compounds with three or more chemical species. Using existing structural search algorithms to examine all possible compositions is not realistic, and the chance to discover desired materials by conventional methods can be extremely low. Complementary high-throughput computational approaches for materials discovery have also been developed. Such approaches can cover a wide range of compositions through exploring a large number of compounds obtained by the substitution of various chemical species into known crystal-structure lattices. Firstprinciples calculations in combination with ML analyses are then performed to identify compounds with desired functionalities. Successful examples of such approaches have been reported in the literature (8-15). A disadvantage of such high-throughput approaches is that most of the substitutional structures are not energetically favorable, and first-principles calculations on these uninteresting structures are costly and ineffective.

An outstanding challenge is to develop a robust strategy to effectively guide a rapid selection of promising compositions that can yield stable crystal structures with targeted physical properties. We develop an ML-guided framework that can efficiently accelerate the discovery of materials, as outlined in Fig. 1. The framework was initiated with an ML model trained using existing first-principles density functional theory (DFT) calculation data from popular public databases. This ML model will provide the rapid prediction of chemical compositions and crystal structures that are likely to exhibit desirable energetic stability (i.e., formation energies) and functionalities. Plausible candidates obtained from the ML screening are validated by first-principles calculations before promising ones are selected for further crystal structure searches using an AGA to discover more lower-energy structures based on the selected chemical compositions. Moreover, new low-energy structures and their properties obtained from AGA and first-principles calculations can be used to adaptively refine the ML model, with the success rate of the prediction improved adaptively.

We demonstrate the efficiency of this ML-guided feedback framework for materials discovery by searching for novel RE-free magnetic materials. Although there have been

Significance

Discovering rare earth (RE)-free magnets that can meet the performance and cost goals for advanced electromagnetic devices has been the dream of many scientists over several decades. We present the efficient discovery and synthesis of an RE-free magnetic Fe₃CoB₂ compound in this paper. Our machine learning (ML)-guided framework greatly reduces the complexity of highthroughput screening and makes ab initio calculations and further structure searches using an adaptive genetic algorithm much more effective than previous approaches. We demonstrate that our ML-guided framework enables the computational discovery and experimental synthesis of an Fe₃CoB₂ compound to be accomplished in days. Our ML-guided framework presents a paradigm for efficient materials design and discovery in the digital era.

Author contributions: W.X. performed the adaptive genetic algorithm structure search; B.B. and D.J.S. synthesized the samples and performed experimental measurement and analysis; B.B., K.-M.H., J.R.C., D.J.S., and C.-Z.W. conceptualized, planned, and coordinated the research; W.X., M.S., B.B., T.L., R.W., C.Z., H.S., K.-M.H., J.R.C., D.J.S., and C.-Z.W. contributed to discussions and analyses of the data; and W.X., M.S., B.B., T.L., R.W., C.Z., H.S., K.-M.H., J.R.C., D.J.S., and C.-Z.W. wrote the paper.

The authors declare no competing interest.

This article is a PNAS Direct Submission.

Copyright © 2022 the Author(s). Published by PNAS. This article is distributed under Creative Commons Attribution-NonCommercial-NoDerivatives License 4.0 (CC BY-NC-ND).

¹To whom correspondence may be addressed. Email: jrc@utexas.edu or wangcz@ameslab.gov.

²Deceased on March 25, 2022.

Published November 14, 2022.

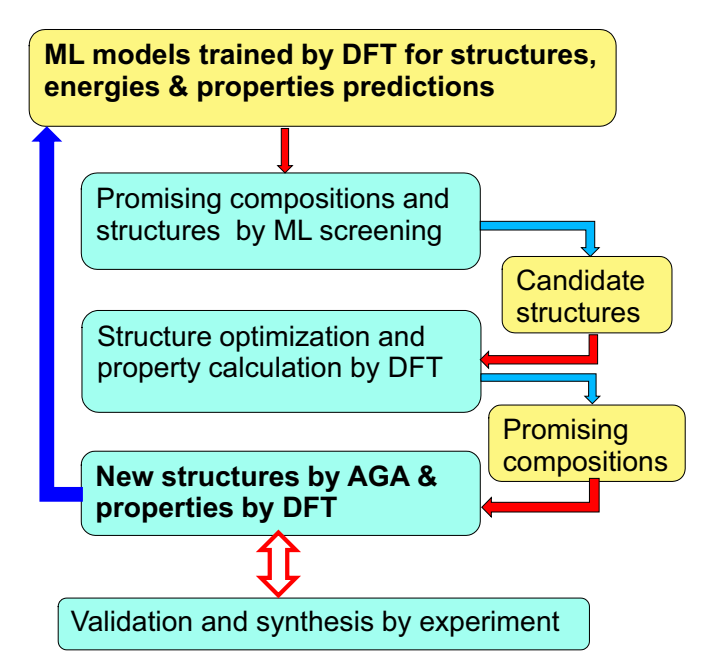


Fig. 1. The ML-guided material discovery framework.

a number of studies on high-throughput calculations in combination with ML for magnetic materials (16-24), an efficient ML-guided framework for greatly accelerating the discovery and synthesis of novel materials is still highly desired. Specifically, we consider an Fe-Co-B system. Our aim is to find new ternary compounds with favorable energetic stability and desired magnetic properties, such as high magnetization and high magnetocrystalline anisotropy energy (MAE), like RE magnets such as Nd₂Fe₁₄B and SmCo₅. Fe-based magnetic materials are attractive, owing to the abundance of Fe and its large atomic magnetic moment. Fe-Co binary alloys are good candidates for ferromagnetic materials. However, they are generally stabilized in cubic structures and exhibit low magnetic anisotropy. Considerable effort has been devoted to combine a third element with Fe and Co to stabilize noncubic ternary structures with a high magnetocrystalline anisotropy. For example, an incorporation of N in FeCo thin films and nanoparticles leads to tetragonal structures with improved magnetocrystalline anisotropies (25, 26). Unfortunately, Fe-Co-N compounds can decompose at higher temperatures of above 500 K (26, 27). The synthesis of bulk Fe-Co-N compounds remains challenging and has yet to be realized. Binary or ternary compounds formed by combining Fe, Co, or FeCo with transition metals such as Zr, Hf, Ti, and Nb also exhibit appreciable magnetocrystalline anisotropies, but their saturation magnetizations are significantly reduced compared to those of Fe and Co (5, 7). For the Fe-Co-B system, no stable ternary structures with desired magnetic properties for permanent-magnet applications have been discovered.

Prior to performing an AGA search, we utilize an ML model to select promising compositions for stable magnetic Fe-Co-B ternary compounds. Our ML model provides a rapid screening over a wide range of possible compositions and crystalline structures to select chemical compositions and crystal structures with desirable formation energies. Consequent DFT optimizations based on the short list of candidate structures selected by ML screening provides information on the magnetic properties of the candidate structures. Here, we adopt the crystal graph convolutional neural network (CGCNN) method (28). In CGCNN, a crystal structure is represented by a crystal graph that encodes both atomic

information and bonding interactions between atoms. A CNN is added on top of the crystal graph to construct the proper descriptors, which are optimal for predicting target properties. In this way, composition-structure-property relationships can be efficiently learned and predicted by CGCNN. The training data in CGCNN are primarily generated by first-principles calculations, which enables a sufficient volume for the supervision training.

We first adopt the parameters in the CGCNN model developed for formation energy predictions of compounds (28). This CGCNN model was trained by using the available structures and DFT-calculated formation energies of 28,046 structures from the Materials Project (MP) database (29). We refer to this model as the first-generation (1G) CGCNN model. We then extract 11,916 known ternary structures from the MP database and replace the three elements with Fe, Co, and B to predict the formation energies of ternary Fe-Co-B compounds using the CGCNN ML model. There are six ways to shuffle the order of three elements into a given ternary structure. We also allow the volume of the crystals to vary by a scaling factor between 0.96 and 1.04 with an interval of 0.02. Therefore, a total of 357,480 hypothetical Fe-Co-B structures are investigated by CGCNN. Noting that the CGCNN model does not have the interatomic forces to relax the bond lengths of the structure, the use of a scaling factor for the volume here allows the CGCNN model to differentiate the energetic stability of the same structure with different bond lengths. The formation energy distribution from the 1G CGCNN prediction for this set of structures is shown in Fig. 2A, where our CGCNN screening suggests that 435 Fe-Co-B structures have negative formation energies. After removing very similar structures, 400 structures from this short list are selected for subsequent DFT calculations.

We also train a CGCNN ML model specifically for predicting Fe-Co-based ternary compounds using DFT formation energies of the 400 Fe-Co-B structures from the 1G CGCNN model and those of 3,469 Fe-Co-X (X = C, N, Si, and S) ternary structures from our magnetic materials database (30). We refer to this CGCNN model as the second-generation (2G) CGCNN model. We apply the 2G CGCNN model to the set of 357,480 structures generated from the MP database discussed above and to another set of 12,755 ternary structures generated by a random generation algorithm (31). The formation energy distribution from the 2G-CGCNN model on these two sets of structures are shown in Fig. 2 B and C, respectively. Additional 2,125 structures that have negative formation energies from the 2G-CGCNN ML model are selected for subsequent DFT structure optimizations. We note that the existing FeCoB, FeCoB₂, and Fe₃Co₃B₂ compounds reported in previous work (32) and the FeCo2B compound in an earlier study (33) are all captured from our 1G and 2G-CGCNN predictions.

After carrying out DFT structure optimizations, we obtain 147 and 570 fully relaxed distinct Fe-Co-B structures from the 1G- and 2G-CGCNN screening, respectively. These 717 structures cover 175 different Fe-Co-B compositions.

We note that the formation energy \bar{E}_f used in the CGCNN is defined with respect to the elementary Fe, Co, and B crystal phases. A negative (positive) formation energy means that the structure is unlikely (likely) to be decomposed into the three elementary crystalline phases. To further assess the energetic stability of the relaxed structures at different compositions, the DFT formation energy with respect to the known convex hull (denoted as E_{hull}) is also calculated for the CGCNN-predicted 717 ternary structures, as shown in Fig. 3A. The E_{hull} of any given phase on the ternary convex hull is calculated by comparing its formation energy with respect to the nearby three known

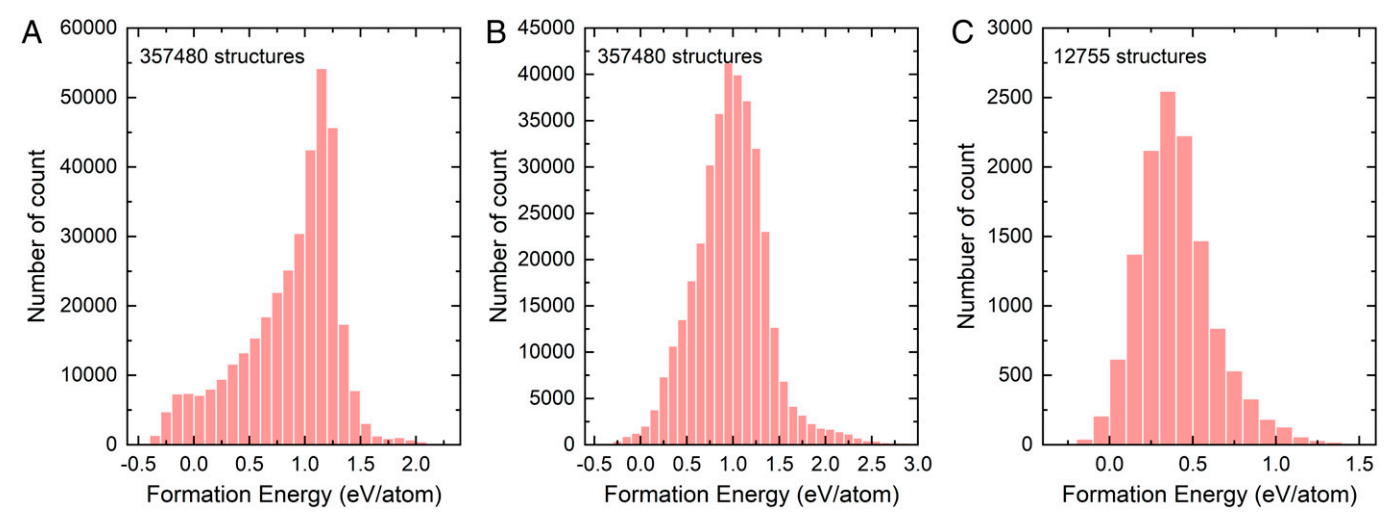


Fig. 2. Formation energy distribution from our CGCNN ML predictions. (*A*) Formation energies from the 1G CGCNN ML model for structures generated using the MP database. (*B*) Formation energies from the 2G CGCNN ML model for structures generated from the MP database. (*C*) Formation energies from the 2G CGCNN ML model for structures generated by random space groups.

phases on the convex hull (ternary, binary, or elementary crystal-line phases), and the chemical compositions of these three phases are located at the vertexes of a triangle (the Gibbs triangle), which enclose the composition of the phase of which E_{bull} is being calculated. We use E_{bull} to assess the thermodynamic stability of the given phase against decomposition into the nearby three known phases.

We can see from Fig. 3A that many of these Fe-Co-B ternary structures exhibit a formation energy very close to the convex hull. Such energetically favorable metastable structures could be synthesized by experiments using nonequilibrium synthesis methods. In Fig. 3B, we also show the magnetization of these structures from DFT calculations.

In the present study, only ferromagnetic configurations are used for the DFT calculations. This should be a reasonable choice used to quickly select promising candidate structures for permanent magnets. The magnetic polarization is obtained by dividing the total magnetic moment in the unit cell from the DFT calculations by the volume of the unit cell. Many of these structures, especially those with rich Fe or/and Co compositions, exhibit high magnetization J_s larger than 1 T.

To assess which structure has both favorable energetic stability and magnetization, we construct a scatterplot with magnetization shown as the horizontal axis and formation energy with respect to the convex hull as the vertical axis (Fig. 3*C*). From ML screening with the CGCNN models we discover 36 promising

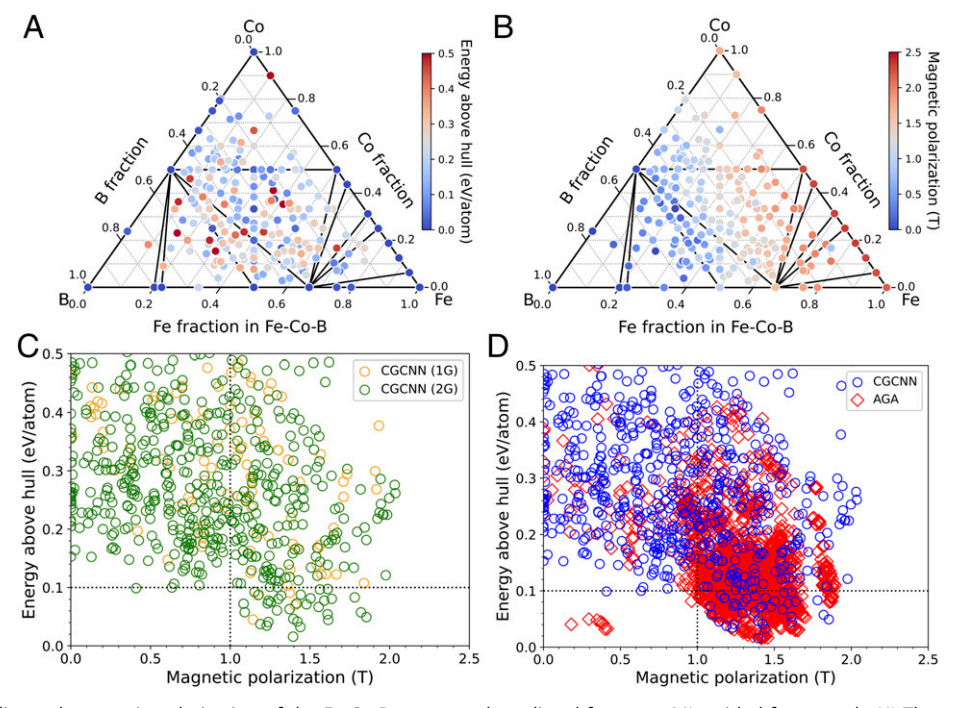


Fig. 3. Energetic stability and magnetic polarization of the Fe-Co-B compound predicted from our ML-guided framework. (A) The energy distance from the convex hull, E_{hull} , and (B) magnetic polarization for the 717 DFT optimized structures selected from the two generations of CGCNN ML models. These structures cover 175 Fe-Co-B compositions. (C) DFT formation energy above the convex hull versus the magnetic polarization, J_s , for structures from the 1G and 2G CGCNN models. Dotted lines indicate the region of interest ($E_{hull} \le 0.1$ eV/atom and $J_s \ge 1$ T). (D) DFT results of E_{hull} and J_s for the structures from two generations of CGCNN models (blue) are compared with those for the structures obtained by AGA (red).

structures ($E_{hull} \le 0.1$ eV/atom and $J_s \ge 1$ T) in Fig. 3C (Right, Bottom) based on the results from DFT calculations.

We also find that the 36 promising structures predicted with the guidance from CGCNN cover 22 compositions out of 175 compositions examined by CGCNN. We therefore select these 22 compositions for further investigation by AGA, thus substantially narrowing the number of compositions to be explored in AGA searches. Based on the 22 compositions, we generate 1,817 structures using AGA. After DFT optimizations, we obtain 557 new metastable structures with $E_{hull} \le 0.1 \text{ eV/atom}$ and a high magnetization, $J_s \ge 1$ T, as shown in Fig. 3D. Compared to 36 structures discovered through ML screening as discussed in the paragraph above, more new promising structures are discovered by AGA, as shown in Fig. 3D. Therefore, with the guidance from ML to select promising compositions, AGA plays an important role in discovery of novel materials in our framework. With our combined ML+AGA+DFT approach, we can efficiently retrieve almost every possible lowenergy structure over a wide range of compositions in this ternary system. As shown in Fig. 3D, we discover 593 Fe-Co-B structures with $E_{hull} \le 0.1$ eV/atom. Such low-energy metastable structures could be synthesized by experimentation, especially under nonequilibrium synthesis conditions. Moreover, more than 90% of the AGA-derived structures have a high magnetization ($J_s \ge 1 \text{ T}$).

We perform DFT calculations with the spin-orbit interactions to estimate the MAE for noncubic structures from the candidate 593 structures with $E_{hull} \le 0.1$ eV/atom and $J_s \ge 1$ T. As discussed above, among these 593 structures, 36 are from CGCNN and 557 are from AGA. We find that seven structures possess a large MAE of $K_1 > 1$ MJ/m³. Among them, three compounds (shown in Fig. 4 C, D, and F) are from the CGCNN prediction and four compounds including the best Fe₃CoB₂ (shown in Fig. 4 A, B, E, and G) are found by the AGA searches. Six of them have a tetragonal or orthorhombic lattice, exhibiting uniaxial anisotropy. Uniaxial anisotropy plays a key role in yielding magnetic coercivity, a measure of a resistance to being demagnetized. The seven Fe-Co-B structures predicted from our scheme have an MAE substantially larger than that of hexagonal close packed Co (0.44 MJ/m³), which is favorable for permanent-magnet applications. In particular, as shown in Fig. 4 and Table 1, the Fe₃CoB₂ compound exhibits the lowest formation energy above the convex hull (22.8 meV/atom) as compared to other high-MAE compounds. The Fe₃CoB₂ compound is an orthorhombic structure with a space group *Cmmm* and lattice parameters of a = 4.211, b = 7.078, and c = 7.149 Å, as schematically shown in Fig. 4A. We performed phonon dispersion calculations for this structure. Our results indicate that the structure is dynamically stable.

To validate and verify our theoretical findings, we employ a nonequilibrium technique involving a rapid quenching of molten alloys to fabricate the new Fe₃CoB₂ compound (see Materials and Methods), which exhibits comparatively lower energy above the convex hull as mentioned in the paragraph above. The experimental X-ray diffraction (XRD) pattern of the Fe₃CoB₂ compound is compared with the simulated XRD pattern of the orthorhombic structure noted in the paragraph above as shown in Fig. 5A. The positions and intensities of the experimental XRD peaks are in good agreement with the calculated ones. We confirm the formation of the predicted Fe₃CoB₂ compound with the orthorhombic structure. Fig. 5B shows the fielddependent magnetization measured at 10 K, which indicates a high J_s for the new compound as predicted by theory, along with a coercivity of $H_c = 0.22$ kOe (Fig. 5B, Inset). We have used the law-of-approach-to-saturation method to determine the magnetic anisotropy constant K_1 and the saturation magnetization M_s (34). By following this approach, we fit the magnetization data measured at 10 K and 300 K near saturation (M_s) in the field range of 30 to 70 kOe using the equation $M=M_{\rm s}$ $(1 - A/H^2) + \chi H$ as shown in the inset of Fig. 5B, where χ is the high-field susceptibility and the constant A depends on K_1 as given by $A = \frac{4}{15} \frac{K_1^2}{M_s^2}$. This analysis yields $K_1 = 1.0$ MJ/m³ and $J_{\rm s} = 1.35 \text{ T at } 300 \text{ K and } K_{\rm 1} = 1.2 \text{ MJ/m}^3 \text{ and } J_{\rm s} = 1.39 \text{ T at}$ 10 K, which are in excellent agreement with the calculated values of $K_1 = 1.34 \text{ MJ/m}^3$ and $J_s = 1.40 \text{ T}$, respectively.

Our results demonstrate that the theoretical guidance by an ML-assisted material search and DFT calculations are crucial in accelerating materials discovery. Our approach quickly identifies magnetic compounds with desired magnetic properties and avoids a time-consuming and expensive experimental optimization process. The room-temperature magnetic properties of Fe_3CoB_2 ($K_1 = 1.0 \text{ MJ/m}^3 \text{ and } J_s = 1.35 \text{ T}$) yield an anisotropy field of $H_a = 2K_1/M_s = 1.86$ T. For potential permanentmagnet materials, Hirayama et al. have proposed that the anisotropy field $(B_a = \mu_0 H_a)$ must be larger than 1.35 I_s by

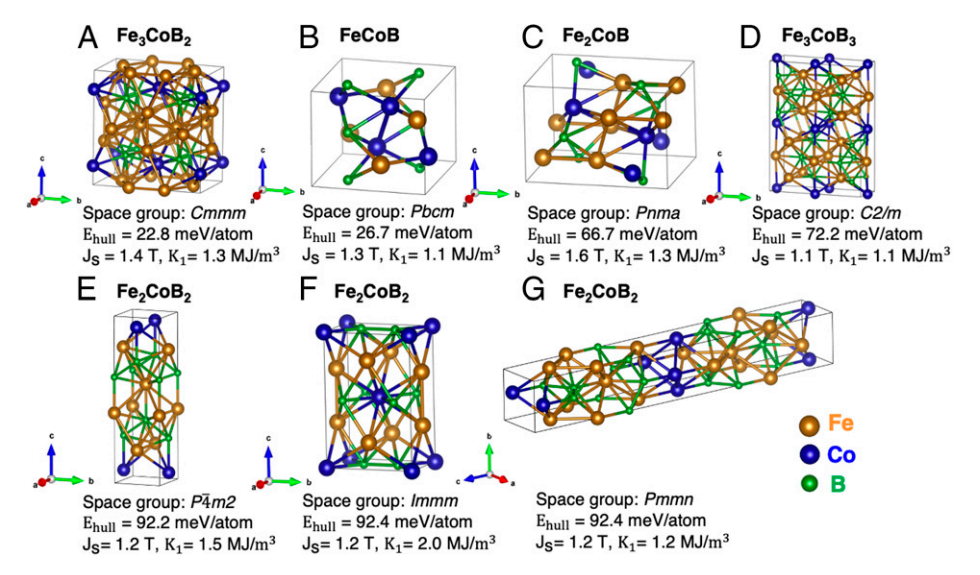


Fig. 4. The crystal structures of seven promising Fe-Co-B compounds for permanent magnet obtained from our ML-AGA-DFT predictions. Among these seven structures, four compounds (A) (B) (E) (G) are discovered by AGA searches, and three compounds (C) (D) (F) are obtained in the ML screening.

Table 1. Space group, formula units per unit cell [Z], formation energy $[E_f]$, E_{hull} , and magnetic properties (magnetic polarization $[J_s]$, magnetic anisotropy energy $[K_1]$, magnetic easy axis, and T_c) of the seven promising Fe-Co-B compounds discovered through our combined ML-AGA-DFT scheme.

Formula	Space Group (No.)	Ζ	E _f		Magnetic Properties			
			$E_{\rm f}$ (meV/atom)	$E_{\rm hull}$ (meV/atom)	$J_s(T)$	K_1 (MJ/m ³)	Easy Axis	$T_{c}(K)$
Fe	Im3m (229)	1	0	0	2.15			1043
Co	$P6_3/mmc$ (194)	2	0	0	1.81	0.41	С	1388
Fe ₃ CoB ₂ [Fig. 4B]	Cmmm (65)	4	-283.7	22.8	1.40	1.34	а	1252
FeCoB [Fig. 4B]	Pbcm (57)	4	-274.1	26.7	1.34	1.07	С	928
Fe ₂ CoB [Fig. 4C]	Pnma (62)	4	-180.3	66.7	1.55	1.32	b	881
Fe ₃ CoB ₃ [Fig. 4D]	C2/m (12)	4	-288.2	72.2	1.08	1.12	С	643
Fe ₂ CoB ₂ [Fig. 4 <i>E</i>]	Immm (71)	2	-258.4	92.4	1.15	1.96	b	789
Fe ₂ CoB ₂ [Fig. 4F]	Pmmn (59)	2	-258.4	92.4	1.25	1.24	С	997
Fe ₂ CoB ₂ [Fig. 4G]	P4m2 (115)	4	-257.8	92.9	1.22	1.48	С	870

Crystallographic data, such as lattice constants and atomic coordinates, of these compounds can be found in the Magnetic Materials Database (30). For comparison, experimental data for bcc Fe and hcp Co are given in italics.

considering intrinsic B_a and nanostructural details (35). Such materials may exhibit energy products as high as J^2 _s/4, if appropriate nanostructuring and alignment of grains are achieved. Fe₃CoB₂ fulfills the above-mentioned criteria for the anisotropy field $(B_a > 1.35 J_s)$. Thus, the new compound or its modification will be important for next-generation critical-materials issues in energy systems.

In summary, we illustrate an effective feedback loop through a combination of ML, AGA, and first-principles DFT calculations. The efficient ML screening provides fast predictions of promising chemical compositions and crystal structures. The subsequent DFT calculations and AGA search yield a good estimation for the energetic stability and magnetic properties of candidate structures. This combination enables efficient materials discovery with desirable stability and properties by experiments. We note that our ML-guided approach is different from common high-throughput approaches in the literature (9, 13, 15, 36) in two aspects. First, in our approach, the highthroughput screening is done much faster with an efficient ML model. Only a small fraction of the structures are checked by first-principles calculations to provide the promising compositions for AGA search. Another notable advantage of our approach is that new structures (beyond known structures) are continuously added to the structure pool by the AGA search. The feedback from AGA is critical since AGA can provide relevant new structures to significantly increase the likelihood for the new materials discovery, especially for ternary and quaternary compounds where available structures from known databases are limited.

Only 2,525 structures (which is less than 0.7% of the total structures screened by ML) predicted by ML and 1,817 structures by AGA are required to be optimized by DFT calculations. According to the timing from our calculations, we estimate that such calculations can be done within a week on a cluster computer of 200 nodes (24-32 cores per node). Our approach efficiently discovered seven Fe-Co-B ternary compounds suitable for permanent-magnet applications. Among them, the lowest-energy Fe₃CoB₂ structure has been synthesized by experiment. With the guidance from our computational study that pinpointed the promising composition, it took only a few days to successfully synthesize the new Fe₃CoB₂ compound and characterize the structural and magnetic properties. Our ML-AGA-DFT experimental framework thus provides timely feedback between computation and experiment to greatly accelerate new materials exploration and discovery.

In this work, we chose B with Fe-Co to demonstrate a "proof of principles" of our proposed ML-guided feedback framework. Discovery of RE-free magnetic materials with other elements is also possible and will be investigated in follow-up work. We believe more new structures for this system or other systems can be discovered by further adaptive iterations to refine our ML model using this framework. We also note that further understanding regarding why Fe₃CoB₂ can have good energetic stability and high magnetization and magnetic anisotropy will also provide useful insights for accelerating the design and discovery of magnetic materials. In general, magnetization comes from transition metal elements (Fe and Co). Therefore, rich composition in Fe and Co will provide high magnetization. However, the origin of magnetic anisotropy is much more complex. While previous work has endeavored to develop a relationship between composition, crystal structure, and magnetic anisotropy (37, 38), a quantitative theory for making such predictions is lacking. Even with the same composition, the symmetry of the crystalline structure, the arrangement, and the local environment of Fe and Co atoms will have significant impact on the magnetic properties, especially the magnetic anisotropy. Future work including using ML to explore such relationships will be interesting and desirable.

Materials and Methods

Computational Methods. The CGCNN model is built with CNNs on top of a crystal graph consisting of convolutional layers and pooling layers (28). Crystals are converted to crystal graphs with nodes representing atoms in the unit cell and edges representing atom connections. The 1G-CGCNN model is trained using the structures and energies of 28,046 compounds from DFT calculations in the MP database (29) following the instructions provided in previous research (28). The nodes of the crystal graph are represented by nine atomic properties of the elements: group number, period number, electronegativity, covalent radius, valence electrons, first ionization energy, electron affinity, block, and atomic volume. The graph edges are characterized by neighboring bonds for each atom/node. R convolutional layers and L1 hidden layers are built on top of these nodes, resulting in a new graph with each node representing the local environment of each atom. After pooling, a vector representing the entire crystal is connected to L2 hidden layers, followed by the output layer to provide the prediction. The mean absolute error of the validation for the 1G-CGCNN model is 0.039 eV/atom. The 1G-CGCNN model is used to perform the screening of the hypothetical structures as described in the main text. Then the 2G-CGCNN model is trained based on the DFT formation energies for the structures from 1G screening and from those Fe-Co-based structures from our magnetic materials database (30) as discussed in the main text. The dataset is divided into a training set

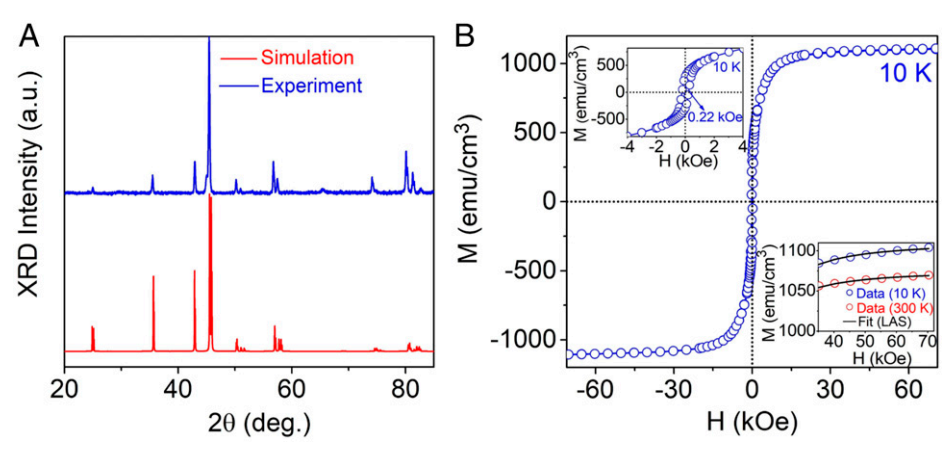


Fig. 5. Structural and magnetic properties of Fe₃CoB₂. (A) A comparison of the experimental XRD pattern with the simulated diffraction pattern of the predicted orthorhombic structure (a.u. stands for atomic unit). (B) Field-dependent magnetization curve measured at 10 K, where the top inset is the corresponding enlarged magnetization curve to show coercivity H_c. The bottom inset shows the fitting of experimental magnetization data (open circles) in the high-field region at 300 K and 10 K using the law-of-approach-to-saturation method (lines) (emu stands for electromagnetic unit).

(80%), validation set (10%), and test set (10%), respectively. We perform 40 epochs of the learning process and select the best model as our 2G-CGCNN model, with the lowest mean absolute error of the validation set (0.104 eV/atom) and the test set (0.136 eV/atom).

The DFT calculations are performed using VASP package (39-41). The Perdew-Burke-Ernzerhof function(42) combined with the projector-augmented wave method (43) and a cutoff energy of 500 eV are used. We use a k-point grid with a mesh size of $2\pi \times 0.025 \text{ Å}^{-1}$ generated by the Monkhorst-Pack scheme. This mesh size is fine enough to sample the first Brillouin zone for achieving better k-point convergence (44). On top of self-consistent spin-polarized calculations, we carry out non-self-consistent noncollinear calculations including the spin-orbit coupling effects for MAE calculations (41). When the spin-orbit couplings are taken into account, symmetry operations are completely turned off and we set the spin-quantization axis to be along different directions. MAE is calculated by taking the energy differences between different spin orientations, while the direction with lowest energy is referred as the easy axis; K_1 is then obtained by the energy difference between the easy axis and the axis with the second-lowest energy $E-E_{easy}$. The Curie temperature (T_c) is evaluated within mean-field approximation by taking the energy difference between ferromagnetic (FM) and antiferromagnetic (AFM) configurations via the simple formula $T_c \sim 2 \frac{E_{AFM} - E_{FM}}{3k_B}$ (45).

We employ an AGA (2, 6, 46) to further search for possible lower-energy structures based on the chemical compositions selected from the ML and DFT calculations. In addition to the conventional genetic algorithm (GA) loop, the AGA adds in an adaptive loop to adaptively adjust the auxiliary interatomic potential used in the conventional GA process. The most time-consuming structure relaxation and energy evaluation step in the conventional GA loop is done efficiently by using the auxiliary interatomic potential. The adaptive loop adjusts the auxiliary interatomic potential from iteration to iteration guided by the accurate results from DFT calculations on the structures selected from the previous interaction of the GA search. Only single-point DFT calculations on a small subset of candidate structures obtained from the previous GA loop (using the auxiliary interatomic potential) are needed at each iteration to quide the adjustment of the potential. The auxiliary interatomic potential for the Fe-Co-B system is expressed according to the embedded atom method (47) with some adjustable parameters. Energies, forces, and stresses of these structures from first-principles DFT calculations are used to update the parameters of the auxiliary interatomic potentials by, e.g., the force-matching method with a stochastic simulated annealing algorithm as implemented in the potfit code (48, 49). Another cycle of GA search is then performed using the newly adjusted interatomic potential, followed by the readjustment of the potential parameters, and the AGA iteration process is then repeated. In this way, for a given composition of the Fe-Co-B ternary, the auxiliary interatomic potential can help in fast sampling of the configuration space through GA and expensive DFT calculations are kept at the minimal without losing the accuracy of the structure search.

Experimental Methods. To fabricate the Fe₃CoB₂ compound, appropriate amounts of high-purity Fe, Co, and B elements are melted using a conventional arc-melting process to obtain alloys with a Fe₃CoB₂ composition. The arc-melted alloys are remelted to a molten state in a quartz tube and subsequently ejected onto the surface of a water-cooled rotating copper wheel to form nanocrystalline ribbons of approximate width 2 mm and thickness 40 μm. The cooling rate during the melt-spinning process is of the order 10⁶ K/s, which facilitates the stability of the metastable structures without decomposition or transformation into equilibrium/ground-state structures. The magnetic properties for the Fe₃CoB₂ compound are measured using the superconducting quantum interference device magnetometer from Quantum D.

Data, Materials, and Software Availability. Some study data are available: New crystallographic data and the computational results for Fe-Co-B ternary compounds, such as the formation energy and magnetic properties, obtained from this work is made available to the public through our NovoMag database, https://www.novomag.physics.iastate.edu/structure-database (50). Other data are all included in the manuscript.

ACKNOWLEDGMENTS. The application of the ML-quided framework and AGA to the discovery of the Fe-Co-B ternary magnetic compounds and the synthesis and characterization of the Fe₃CoB₂ compound were supported by the NSF through the Designing Materials to Revolutionize and Engineer our Future program with award numbers 1729202, 1729677, and 1729288. The development of the ML-guided framework and AGA method was supported by the U.S. Department of Energy Office of Science, Basic Energy Sciences, Materials Science and Engineering Division under contract number DE-AC02-07CH11358, including the computer time allocation at the National Energy Research Scientific Computing Center in Berkeley, CA. Renhai Wang acknowledges support from the Guangdong Natural Science Foundation of China (grant nos. 2017B030306003 and 2019B1515120078). Chao Zhang was supported by the National Natural Science Foundation of China (grant nos. 11874318 and 11774299). High performance computing (HPC) resources resources were provided by the Texas Advanced Computing Center through the Extreme Science and Engineering Discovery Environment allocation. HPC resources were also provided by the Supercomputer Center at the Institute for Solid State Physics at the University of Tokyo. Research at the University of Nebraska is partly performed in the Nebraska Nanoscale Facility: National Nanotechnology Coordinated Infrastructure and at the Nebraska Center for Materials and Nanoscience, which are supported by the NSF under award ECCS 2025298 and the Nebraska Research Initiative.

Author affiliations: ^aDepartment of Physics and Astronomy, Iowa State University, Ames, IA 50011; ^bAmes Laboratory, U.S. Department of Energy, Iowa State University, Ames, IA 50011; ^cCenter for Computational Materials, Oden Institute for Computational Engineering and Sciences, The University of Texas at Austin, Austin, TX 78712; ^dThe Institute for Solid State Physics, The University of Tokyo, Kashiwa, Chiba 277-8581, Japan; ^eNebraska Center for Materials and Nanoscience, University of Nebraska, Lincoln, NE 68588; Department of Physics and Astronomy, University of Nebraska,

Lincoln, NE 68588; ⁸Department of Physics, The University of Texas at Austin, Austin, TX 78712; ^hSchool of Physics and Optoelectronic Engineering, Guangdong University of Technology, Guangzhou 510006, China; Department of Physics, Yantai University,

- D. M. Deaven, K. M. Ho, Molecular geometry optimization with a genetic algorithm. Phys. Rev. Lett. 75, 288-291 (1995).
- S. Q. Wu et al., An adaptive genetic algorithm for crystal structure prediction. J. Phys. Condens. Matter 26, 035402 (2014).
- D. E. Goldberg, J. H. Holland, Genetic algorithms and machine learning. Mach. Learn. 3, 95-99
- D. C. Lonie, E. Zurek, XtalOpt: An open-source evolutionary algorithm for crystal structure prediction. Comput. Phys. Commun. 182, 372-387 (2011).
- B. Balamurugan, B. Das, W. Y. Zhang, R. Skornski, D. J. Sellmyer, Hf-Co and Zr-Co alloys for rare-earth-free permanent magnets. *J. Phys. Condens. Matter* **26**, 064204 (2014).
- X. Zhao et al., Exploring the structural complexity of intermetallic compounds by an adaptive genetic algorithm. Phys. Rev. Lett. 112, 045502 (2014).
- B. Balasubramanian *et al.*, Synergistic computational and experimental discovery of novel magnetic materials. *Mol. Syst. Des. Eng.* **5**, 1098–1117 (2020).

 J. E. Saal, S. Kirklin, M. Aykol, B. Meredig, C. Wolverton, Materials design and discovery with
- high-throughput density functional theory: The open quantum materials database (OQMD). JOM **65**, 1501-1509 (2013).
- G. R. Schleder, A. C. M. Padilha, C. M. Acosta, M. Costa, A. Fazzio, From DFT to machine learning: Recent approaches to materials science-a review. Journal of Physics: Materials 2, 032001 (2019).
- W. Chen, "High-throughput computing for accelerated materials discovery" in Computational Materials System Design, D. Shin, J. Saal, Eds. (Springer International Publishing, Cham, Switzerland, 2018), pp. 169-191.
- L. Himanen, A. Geurts, A. S. Foster, P. Rinke, Data-driven materials science: Status, challenges, and perspectives. Adv. Sci. (Weinh.) 6, 1900808 (2019).
- S. Curtarolo et al., AFLOW: An automatic framework for high-throughput materials discovery. Comput. Mater. Sci. 58, 218-226 (2012).
- J. Cai, X. Chu, K. Xu, H. Li, J. Wei, Machine learning-driven new material discovery. Nanoscale Adv. 2, 3115-3130 (2020).
- J. E. Gubernatis, T. Lookman, Machine learning in materials design and discovery: Examples from
- the present and suggestions for the future. Phys. Rev. Mater. 2, 120301 (2018). R. Vasudevan, G. Pilania, P. V. Balachandran, Machine learning for materials design and discovery.
- J. Appl. Phys. 129, 070401 (2021). A. G. Kusne *et al.*, On-the-fly machine-learning for high-throughput experiments: Search for rare-earth-free permanent magnets. *Sci. Rep.* **4**, 6367 (2014).
- A. Kabiraj, M. Kumar, S. Mahapatra, High-throughput discovery of high Curie point two
- dimensional ferromagnetic materials. npj Comput. Mater. 6, 35 (2020). D. Torelli, H. Moustafa, K. W. Jacobsen, T. Olsen, High-throughput computational screening for two-dimensional magnetic materials based on experimental databases of three-dimensional compounds. npj Comput. Mater. 6, 158 (2020).
- 19. H. Zhang, High-throughput design of magnetic materials. Electronic Structure 3, 033001 (2021).
- G. Katsikas, S. Charalampos, K. Joseph, Machine learning in magnetic materials. Phys. Status Solidi (b) 258, 2000600 (2021).
- T. D. Rhone et al., Data-driven studies of magnetic two-dimensional materials. Sci. Rep. 10, 15795 (2020).
- G. A. Landrum, H. Genin, Application of machine-learning methods to solid-state chemistry: Ferromagnetism in transition metal alloys. J. Solid State Chem. 176, 587-593 (2003).
- I. Miyazato, Y. Tanaka, K. Takahashi, Accelerating the discovery of hidden two-dimensional magnets using machine learning and first principle calculations. J. Phys. Condens. Matter 30, 06LT01 (2018).
- S. Arapan, P. Nieves, S. Cuesta-López, A high-throughput exploration of magnetic materials by using structure predicting methods. *J. Appl. Phys.* **123**, 083904 (2018).
- T. Hasegawa, T. Niibori, Y. Takemasa, M. Oikawa, Stabilisation of tetragonal FeCo structure with high magnetic anisotropy by the addition of V and N elements. Sci. Rep. 9, 5248 (2019).

Yantai 264005, China; ^JDepartment of Physics, Zhejiang Agriculture and Forestry University, Zhuji 311800, China; and ^kMcKetta Department of Chemical Engineering, The University of Texas at Austin, Austin, TX 78712

- 26. X. Zhao et al., Large magnetic anisotropy predicted for rare-earth-free Fe_{16-x}Co_xN₂ alloys. Phys. Rev. B 94, 224424 (2016).
- M. Takahashi et al., Magnetic moment of α'' -Fe16N2 films (invited). J. Appl. Phys. **76**, 6642-6647
- 28. T. Xie, J. C. Grossman, Crystal graph convolutional neural networks for an accurate and interpretable prediction of material properties. Phys. Rev. Lett. 120, 145301 (2018).
- A. Jain et al., Commentary: The Materials Project: A materials genome approach to accelerating materials innovation. APL Mater. 1, 011002 (2013).
- M. Sakurai et al., Discovering rare-earth-free magnetic materials through the development of a database. Phys. Rev. Mater. 4, 114408 (2020).
- P. Avery, E. Zurek, RandSpg: An open-source program for generating atomistic crystal structures with specific spacegroups. *Comput. Phys. Commun.* **213**, 208–216 (2017).
- G. Pradelli, C. Gianoglio, E. Quadrini, Il Sistema Cobalto-Ferro-Boro in Presenza Di Liquido. *Metall. Ital.; Ita; Da.* **73**, 351–362. (1981).
- D. Fruchart, P. Chaudouet, R. Fruchart, A. Rouault, J. P. Senateur, Etudes structurales de composés de type cémentite: Effet de l'hydroge'ne sur Fe₃C suivi par diffraction neutronique. Spectrométrie Mössbauer sur FeCo₂B et Co₃B dopés au³⁷Fe. *J. Solid State Chem.* **51**, 246-252
- G. Hadjipanayis, D. J. Sellmyer, B. Brandt, Rare-earth-rich metallic glasses. I. Magnetic hysteresis. Phys. Rev. B 23, 3349-3354 (1981).
- Y. Hirayama, T. Miyake, K. Hono, Rare-earth lean hard magnet compound NdFe₁₂N. JOM 67, 1344-1349 (2015).
- D. Jha et al., Enhancing materials property prediction by leveraging computational and experimental data using deep transfer learning. Nat. Commun. 10, 5316 (2019).
- Y. Xie, G. A. Tritsaris, O. Grånäs, T. D. Rhone, Data-driven studies of the magnetic anisotropy of twodimensional magnetic materials. J. Phys. Chem. Lett. 12, 12048-12054 (2021).
- P. Larson, I. I. Mazin, D. A. Papaconstantopoulos, Calculation of magnetic anisotropy energy in SmCo₅. Phys. Rev. B 67, 214405 (2003).
- G. Kresse, J. Furthmüller, Efficiency of ab-initio total energy calculations for metals and semiconductors using a plane-wave basis set. *Comput. Mater. Sci.* **6**, 15–50 (1996).
- 40. G. Kresse, J. Furthmüller, Efficient iterative schemes for ab initio total-energy calculations using a plane-wave basis set. Phys. Rev. B Condens. Matter 54, 11169-11186 (1996).
- 41. S. Steiner, S. Khmelevskyi, M. Marsmann, G. Kresse, Calculation of the magnetic anisotropy with projected-augmented-wave methodology and the case study of disordered Fe_{1-x}Co_x alloys. Phys. Rev. B 93, 224425 (2016).
- J. P. Perdew, K. Burke, M. Ernzerhof, Generalized gradient approximation made simple. Phys. Rev. Lett. 77, 3865-3868 (1996).
- P. E. Blöchl, Projector augmented-wave method. Phys. Rev. B Condens. Matter 50, 17953-17979 (1994).
- M. Sakurai, J. R. Chelikowsky, Real-space pseudopotential method for calculating magnetocrystalline anisotropy. Phys. Rev. Mater. 2, 084411 (2018).
- P. Kurz, G. Bihlmayer, S. Blügel, Magnetism and electronic structure of hcp Gd and the Gd(0001) surface. J. Phys. Condens. Matter 14, 6353-6371 (2002).
- 46. X. Zhao et al., Interface structure prediction from first-principles. J. Phys. Chem. C 118, 9524-9530
- 47. M. S. Daw, M. I. Baskes, Semiempirical, quantum mechanical calculation of hydrogen embrittlement in metals. Phys. Rev. Lett. 50, 1285-1288 (1983).
- 48. P. Brommer, F. Gahler, Effective potentials for quasicrystals from ab-initio data. Philos. Mag. 86, 753-758 (2006).
- P. Brommer, F. Gähler, Potfit: Effective potentials from ab initio data. *Model. Simul. Mater. Sci.* Eng. 15, 295-304 (2007).
- J. R. Chelikowsky, K.-M. Ho, C.-Z. Wang, D. J. Sellmyer, X. Xu, Fe-Co-B ternary compounds. NovoMag. https://www.novomag.physics.iastate.edu/structure-database. Accessed 19 October